Chinese Chemical Letters 37 (2026) 111532

Contents lists available at ScienceDirect

Chinese Chemical Letters

journal homepage: www.elsevier.com/locate/cclet

Ln^{3+}/Bi^{3+}-induced the assembly of molybdenum-oxygen clusters with proton conductivity

Jiajia Li[a,1], Liying Wang[b,1], Qianqian Liu[b], Shuang Yu[b], Hong-Ying Zang[b,*], Zhong-Min Su[a,c,*]

[a] School of Chemistry and Environmental Engineering, Changchun University of Science and Technology, Changchun 130022, China
[b] Key Laboratory of Polyoxometalate and Reticular Material Chemistry of Ministry of Education, Northeast Normal University, Changchun 130024, China
[c] Key Laboratory of Tropical Medicinal Resource Chemistry of Ministry of Education, Hainan Normal University, Haikou 571158, China

ARTICLE INFO

Article history:
Received 28 May 2025
Revised 28 June 2025
Accepted 2 July 2025
Available online 3 July 2025

Keywords:
Polyoxometalates
Rare earth
Molybdenum cluster
Hydrogen bond
Proton conduction

ABSTRACT

The most notable structural features of polyoxometalates (POMs) are their large molecular size and relatively low effective surface charge density. These properties endow POMs with excellent Brønsted acidity and proton mobility, making them ideal materials for proton conductors. In this study, a series of homotrimeric complexes were successfully synthesized through Ln^{3+}/Bi^{3+} induced assembly of a suitable organic ligand 1-hydroxyethylidene 1,1-diphosphonic acid (HEDP): $H_9[La(Mo_2O_4)_6(H_2O)_6(HEDP)_6](LaO_9H_6)\cdot 18H_2O$ (complex **1**), $H_9[Nd(Mo_2O_4)_6(H_2O)_6(HEDP)_6](NdO_6H_{12})\cdot 15H_2O$ (complex **2**), and $H_9[Bi(Mo_2O_4)_6(H_2O)_6(HEDP)_6]$ (complex **3**). Notably, the presence of free rare earth ions in the asymmetric unit of complexes **1** and **2** is a structural feature that results in a tighter hydrogen-bonding network in their three-dimensional stacking structures, which in turn significantly enhances the proton conductivity. Complexes **1**–**3** exhibit excellent proton conductivity, with measured values of 3.35×10^{-2}, 3.81×10^{-2}, and 2.37×10^{-2} S/cm under 98% relative humidity at 80 °C. This study establishes a promising strategy for designing molybdate cluster-based materials with enhanced proton conduction properties.

© 2026 Published by Elsevier B.V. on behalf of Chinese Chemical Society and Institute of Materia Medica, Chinese Academy of Medical Sciences.

Fuel cells, especially proton exchange membrane fuel cells (PEMFCs), are a promising clean energy source [1–6]. The proton exchange membrane (PEM) in PEMFCs requires high proton conductivity and chemical stability [7–11]. Although Nafion membranes are widely used for their high conductivity, they lose this property over time at high temperatures and are expensive [12–16]. To overcome these limitations, alternative electrolytes such as liquid crystals, inorganic oxides, and organic-inorganic hybrid materials have been investigated for enhancing ionic conductivity, thermal stability, and durability [17,18]. Furthermore, organic-inorganic hybrid materials can be effective electrolytes, facilitating ion/proton transport while improving conductivity and stability [19–21].

Polyoxometalates (POMs) are considered to be a highly promising class of proton conducting materials due to their low effective surface charge density, excellent thermal stability, outstanding electron acceptance, and discrete mobile ions [22–26]. POMs show unique advantages in the preparation of proton conducting materials: Firstly, the oxygen atoms on the surface of POMs can act as proton hopping sites [27–29]; Secondly, POMs can be precisely tuned at the molecular level, thus enabling efficient proton transport pathways [30–34]; Finally, POMs exhibit strong Brønsted acidity and contain multiple protons (H^+) or hydrogen-based counterions in their structure, earning them the name 'proton pump' [35].

To enhance material properties, particularly proton conductivity, researchers often incorporate organic groups into the material design. These organic groups can either be covalently bonded to POM frameworks or serve as counterions to form electrostatic complexes with polymers [36–38]. Using this strategy, we achieved precise modulation of the microstructure of the material and significantly enhanced its chemical stability and physical properties. In this study, a series of crystalline materials with excellent proton conductivity were successfully constructed by introducing the synergistic assembly of phosphate ligands and metal ions. Notably noteworthy is that the three-dimensional hydrogen bonding network structure formed between the H and O atoms of the organic ligands and the POMs provide the complexes with efficient proton

* Corresponding authors.
E-mail addresses: zanghy100@nenu.edu.cn (H.-Y. Zang), zmsu@nenu.edu.cn (Z.-M. Su).
[1] These authors contributed equally to this work.

https://doi.org/10.1016/j.cclet.2025.111532
1001-8417/© 2026 Published by Elsevier B.V. on behalf of Chinese Chemical Society and Institute of Materia Medica, Chinese Academy of Medical Sciences.

transport channels, thus significantly enhancing their proton conductivity [39–43].

Therefore, exploring new organic ligand-functionalized POMs with hydrogen-bonding networks is crucial for advancing POMs chemistry. Inspired by these results, we designed and synthesized a series of polymolybdates $H_9[La(Mo_2O_4)_6(H_2O)_6(HEDP)_6](LaO_9H_6)\cdot 18H_2O$ (complex **1**), $H_9[Nd(Mo_2O_4)_6(H_2O)_6(HEDP)_6](NdO_6H_{12})\cdot 15H_2O$ (complex **2**), and $H_9[Bi(Mo_2O_4)_6(H_2O)_6(HEDP)_6]$ (complex **3**). Complexes **1**–**3** all utilize the phosphonic acid moiety of the polydentate phosphonate ligand for covalent modification of the $\{Mo_2O_{10}\}$ moiety. In addition, these complexes feature an integrated hydrogen bonding network. Interestingly, under the same experimental conditions, the difference between rare earth ions (La^{3+}, Nd^{3+}) and bismuth (Bi^{3+}) leads to differences in the stacking structures, which in turn affect their proton conductivity properties. Specifically, complexes **1** and **2** contain a free Ln^{3+} in the asymmetric unit, whereas no free Bi^{3+} ions is present in complex **3**. This structural difference leads to the formation of a tighter hydrogen bonding network in the stacking structure of complexes **1** and **2**, which significantly enhances their proton conductivity to 1.41 and 1.61 times that of complex **3**, respectively. The proton conductivity tests reveal that complexes **1**–**3** are excellent proton-conducting materials with values of 3.35×10^{-2}, 3.81×10^{-2}, and 2.37×10^{-2} S/cm at 353 K and 98 % relative humidity (RH).

$(NH_4)_6Mo_7O_{24}\cdot 4H_2O$, $NH_2NH_2\cdot 2HCl$, $CoSO_4\cdot 7H_2O$, $LaCl_3\cdot 5H_2O$ were acidified by HEDP under hydrothermal reaction to produce pure orange needle crystals. In addition, under the same conditions **2** and **3** can be obtained by replacing $LaCl_3$ with $NdCl_3\cdot 5H_2O$, $BiCl_3\cdot 5H_2O$, respectively. Detailed synthesis procedures are in Supporting information.

Single-crystal X-ray structural analyses reveal that complexes **1**–**3** crystallize in the Hexagonal crystal system with the $P6_3/m$ space group (Table S1 in Supporting information). Notably, the asymmetric units of complexes **1** and **2** comprise an anionic framework and free rare earth ions, whereas complex **3** lacks free ions. A detailed description of the structure of **3** follows. As shown in Fig. 1, it should be noted that polyoxoanion in complex **3** consists of three $\{Mo_4O_{12}(HEDP)_2\}$ (Fig. 1a) building blocks linked by one $\{BiO_9\}$ dodecahedron (Fig. 1b). The coordination environment of Bi^{3+} is shown in Fig. 1c.

The $\{Mo_4O_{12}(HEDP)_2\}$ building block consists of two edge-sharing $\{Mo_2O_{10}\}$ units linked through their terminal oxygen atoms to the P1 atoms of the $\{PO_3\}$ groups of the two HEDP ligands. The P-O lengths of the $\{PO_3\}$ groups are in the range of 1.506(3)-1.546(3) Å, (Table S2 in Supporting information). The Bi center coordinates to nine oxygen atoms from three distinct $\{Mo_4O_{12}(HEDP)_2\}$ structural units, forming a polyoxoanion (Fig. 1e). Specifically, Bi coordinates with one μ_2-oxo bridge (O4) and two terminal oxo ligands (O5) from a $\{Mo_4O_{12}(HEDP)_2\}$ building block (Fig. 1d). The observed Bi-O bond distances range from 2.474(4) Å to 2.517(3) Å. The highly symmetric anionic framework of complex **3** assembles into an ideal equilateral triangular cluster featuring a central Bi^{3+}. Connecting the three molybdenum atoms at the vertex positions of the triangle cluster results in a perfect equilateral triangle with uniform edge lengths of 10.50 Å (Fig. 1f).

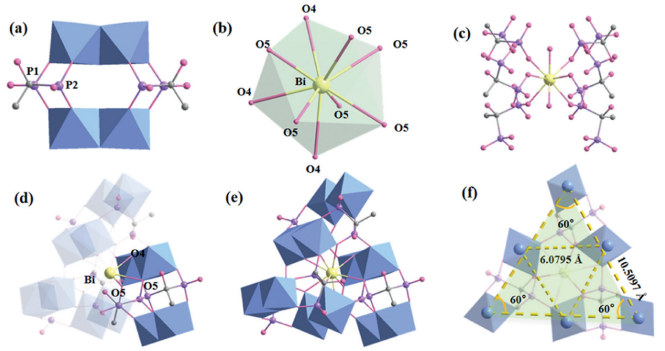


Fig. 1. (a) $\{Mo_4O_{12}(HEDP)_2\}$ unit of the **3.** (b, c) Coordination environments of the Bi^{3+}. (d) Coordination mode of Bi^{3+} with $\{Mo_4O_{12}(HEDP)_2\}$ building blocks. (e) Asymmetric unit of complex **3**. (f) The trimeric structure of **3**, Color scheme for polyhedra: Mo (blue), Bi (yellow), P (purple), C (grey), O (pink).

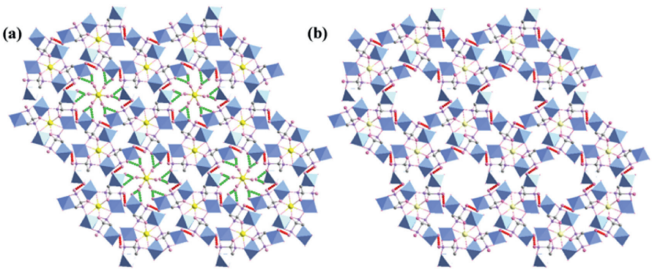


Fig. 2. Schematic diagram of hydrogen bonding in the 3D stacking structure of (a) **1** and (b) **3**. Color scheme for polyhedra: $\{MoO_6\}$ (blue), Bi/La (yellow), P (purple), C (grey), O (pink), O–H···O hydrogen bond (between $\{BiO_9\}$ and $\{Mo_4O_{12}(HEDP)_2\}$), green dashed line; O–H···O hydrogen bond (between HEDP and $\{Mo_4O_{12}(HEDP)_2\}$), red dashed line.

Interestingly, despite the same synthetic conditions and the fact that complexes **1**–**3** shares the same anionic framework (Fig. 1e and Fig. S1), the presence of free Ln^{3+} was observed in the asymmetric units of both complexes **1** and **2**, whereas free Bi^{3+} was absent in complex **3**. This resulted in significant differences in the three-dimensional stacking structures of complexes **1**–**3** (Figs. S2 and S3 in Supporting information). Specifically, the stacking channels of **1** and **2** are filled with free Ln^{3+} in regular rows, whereas the stacking structure of **3** is devoid of free Bi^{3+}. This structural difference directly affects how the hydrogen bonds in complexes **1**–**3** are connected. The $\{PO_3\}$ of the ligand HEDP and the $\{Mo_2O_{10}\}$ of the $\{Mo_4O_{12}(HEDP)_2\}$ unit build a highly ordered and continuous hydrogen bonding network through intermolecular interactions. However, in complexes **1** and **2**, an additional hydrogen-bonding network forms between the free hydrated Ln^{3+} ions in their three-dimensional framework and the terminal oxygen atoms of neighboring $\{Mo_2O_{10}\}$ subunits. In contrast, complex **3** lacks such interactions entirely (Fig. 2). This is also the fundamental reason why complexes **1** and **2** possess a greater abundance of hydrogen bonds than complex **3**, which has been confirmed by Hirschfeld surface analysis.

The Hirschfeld surface analysis of complexes **1** and **3**, depicted in Figs. 3a–f, provides insights into the intermolecular interactions through the use of different color schemes in the d_{norm} and shape index plots [44,45]. The 2D fingerprint plots for **1** indicate an O···H/H···O ratio of 43.5 %, suggesting that there is an abundance of hydrogen bonding interactions between the **1** molecules. Notably, the 2D fingerprint plots of **3** present an O···H/H···O ratio of 35 %, which is 8.5 % lower compared to **1**. These data indicate that the hydrogen bonding in **3** is relatively weak, thus further confirming the aforementioned argument. Through systematic characterisation by powder X-ray diffraction (PXRD), FT-IR and thermogravimetric analysis (TGA) (Figs. S5-S7 in Supporting information), we have comprehensively characterised the phase purity, chemical structure and thermal stability of complexes **1**–**3**. The experimental results show that the PXRD test patterns of complexes **1**–**3** are in high agreement with the theoretical simulation results, fully confirming their excellent phase purity.

The multiple proton transport sites on the inner and outer surfaces of the complexes, as well as the presence of a dense network of hydrogen bonds in their structures, make them excellent candi-

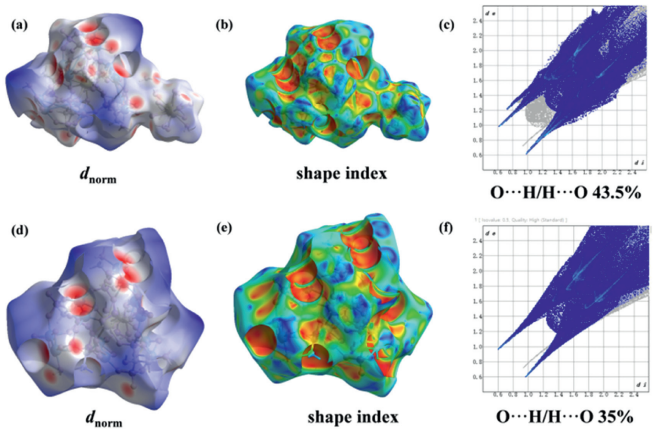


Fig. 3. (a) The d_{norm} map, (b) shape index map and (c) the 2D fingerprint plots of **1**. (d) The d_{norm} map, (e) shape index map and (f) the 2D fingerprint plots of **3**.

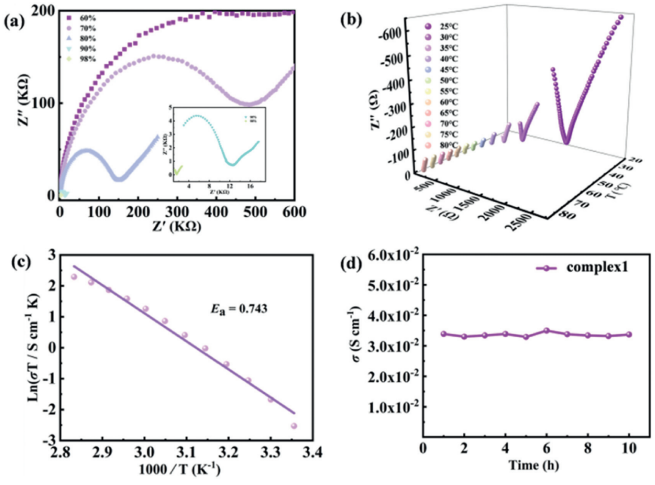


Fig. 4. (a) Nyquist plots of **1** under different RH at 25 °C. (b) Nyquist plots of **1** at 98 % RH under different temperatures. (c) Arrhenius plots and linear fitting of temperature-dependent proton conduction at 98 %RH of **1**. (d) Time-dependent conductivity (σ) at 98 % RH and 80 °C.

dates for molecular-based proton conductors. Therefore, the proton conductivity properties of **1**–**3** were tested at temperatures ranging from 25 °C to 80 °C and humidity ranging from 60 %–98 % RH. The results of the test are shown in Fig. 4 and Fig. S9 (Supporting information). The proton conductivity of the complexes increases considerably with increasing humidity (Fig. 4a, Figs. S9a and d). Suggesting that the proton transport in the structure along the hydrogen bonding network is more efficient at higher relative humidity. For this purpose, the complexes were tested for water vapour adsorption, showing the same increasing trend in the water adsorption isotherm. Fig. S8 (Supporting information) shows that the maximum water vapor adsorption of the complexes **1**–**3** can reach up to 198.5, 152.6 and 185 mg/g, respectively, when the value of P/P_0 is around 0.9. In addition, all the complexes showed similar conductivity at the same RH, due to complexes **1**–**3** belong to isostructure, which leads to the similarity in their proton conduction patterns.

The 98 % RH was selected as the optimum humidity condition at temperatures ranging from 25 °C to 80 °C for further investigation of the proton conductivity properties of the complexes (Fig. 4b and Figs. S9b and e). Their proton conductivity of these complexes increases from 2.83×10^{-4}, 2.34×10^{-4}, and 2.23×10^{-4} S/cm to 3.35×10^{-2}, 3.81×10^{-2}, and 2.37×10^{-2} S/cm, respectively. This increase in conductivity is attributed to the accelerated motion of water molecules at high temperatures [46]. Moreover, complexes **1**–**3** exhibit high σ and possess excellent proton conductivity compared to the proton conductivity of many POMs reported that have been published in recent years (Fig. S13 and Table S4 in Supporting information). The stability of a good proton conductor was identified as a crucial factor for its practical implementation. The stability test of complexes **1**–**3** was carried out at 80 °C and 98 % RH (Fig. 4d and Fig. S10 in Supporting information). The conductivity values remained essentially the same throughout, indicating that complexes **1**–**3** have stable conductivity properties. In addition, the Hebb-Wagner direct current polarization method was used to investigate time-dependent current profiles of **1**–**3**. At a constant voltage of 0.1 V, the resistances of **1**–**3** were 3.7×10^6, 4.97×10^6, and 1.05×10^7 Ω, respectively (Fig. S12 in Supporting information). The results verify that **1**–**3** mainly contribute to proton conduction rather than other ionic conduction.

To gain deeper insights into the proton conduction mechanisms, we systematically investigated the temperature-dependent σ by employing the Arrhenius equation for comprehensive analysis. Two predominant mechanisms govern proton conduction in materials: (1) The vehicular mechanism, characterized by an activation energy (E_a) greater than 0.4 eV, and (2) the Grotthuss mechanism, which exhibits a lower activation energy ($E_a < 0.4$ eV). The activation energy for proton conductionof complex **1** was calculated to be 0.743 eV based on the slope of fitted their conductivities data of Fig. 4c. Similarly, values of 0.762 eV and 0.78 eV were obtained for complexes **2** and **3**, respectively. The close agreement among these activation energy values strongly suggests that proton conduction in all three compounds proceeds follows a vehicular mechanism. After the proton conduction tests were completed, IR and powder X-ray diffraction measurements were performed on complexes **1**–**3**. The diffraction peaks of all three compounds were found to be consistent with those of the original samples (Figs. S4 and S5 in Supporting information), indicating that they maintained their structural integrity.

In the 3D crystal structures of complexes **1**–**3**, the {PO_3} of the ligand HEDP and the {Mo_2O_{10}} unit of {$Mo_4O_{12}(HEDP)_2$} form a highly ordered continuous hydrogen bonding network through hydrogen bonding interactions, which constructs an effective proton transport channel. In addition, the presence of a large number of crystalline water molecules and dissociable hydrogen protons in the structure further facilitates the proton conduction process. Complexes **1**–**3** all exhibit excellent proton conduction performance, which is mainly attributed to the rapid proton migration in the hydrogen bonding network where water molecules act as proton carriers. As shown in Fig. S11 (Supporting information), we propose a model for the possible proton conduction mechanism of complexes **1**–**3**, revealing the constitutive relationship between the water molecule-mediated proton transport process and the structural characteristics of the materials.

Notably, complexes **1** and **2** exhibit higher proton conductivity than **3**, although they are within the same order of magnitude. This is due to the fact that complexes **1** and **2** presence of a free Ln^{3+} in their asymmetric units compared to complex **3**, resulting in the formation of a large number of hydrogen bonds between the coordination water of Ln^{3+} and the {Mo_2O_{10}} unit of {$Mo_4O_{12}(HEDP)_2$}. This allows for easier proton transfer, which significantly improves proton conductivity.

In conclusion, we have formed a series of homotrimeric molybdate clusters by selecting suitable organic ligands and by using Ln^{3+}/Bi^{3+} induced formation. The structures of complexes **1**–**3** were fully characterized, and their proton conduction properties were systematically investigated. Notably, complexes **1** and **2** exhibit significantly higher σ than complex **3**, which we attribute this to differences in the **1**–**3** hydrogen bonding network. All three complexes display super protonic conductivity exceeding

10^{-2} S/cm, demonstrating their potential as high-performance proton-conducting POMs materials. This work not only provides a viable strategy for designing highly proton-conductive POMs but also opens new avenues for the development of advanced proton-conducting materials.

CRediT authorship contribution statement

Jiajia Li: Writing – original draft. **Liying Wang:** Writing – original draft. **Qianqian Liu:** Writing – original draft. **Shuang Yu:** Writing – original draft. **Hong-Ying Zang:** Writing – review & editing. **Zhong-Min Su:** Writing – review & editing.

Declaration of competing interest

The authors declare that they have no known competing financial interests or personal relationships that could have appeared to influence the work reported in this paper.

Acknowledgments

This work was supported by the National Natural Science Foundation of China (Nos. 22322102, 22271023), the Fundamental Research Funds for the Central Universities-Excellent Youth Team Program (No. 2412023YQ001), the Natural Science Foundation of Jilin Province (No. 20200201083JC), the Natural Science Foundation of the Department of Education of Jilin Province (No. JJKH20201169KJ).

Supplementary materials

Supplementary material associated with this article can be found, in the online version, at doi:10.1016/j.cclet.2025.111532.

References

[1] S. Ong, A. Al-Othman, M. Tawalbeh, Energy 277 (2023) 127721.
[2] F. Peng, J.X. Zou, J. Chen, M. Wang, M.B. Wu, J. Power Sources 645 (2025) 237219.
[3] X.L. Sun, G.J. Zhang, J.Q. Fu, D.X. Xi, W.Q. Long, Energy 323 (2025) 135913.
[4] A. Saha, R. Sahoo, S.C. Pal, S. Uchida, M.C. Das, ACS Energy Lett. 10 (2025) 1958–1998.
[5] A. Chitsaz, M.A. Haghghi, J. Hosseinpour, Energy Convers. Manage. 186 (2019) 487–499.
[6] H.Q. Jin, S.Y. Zou, X.C. Zhou, et al., Chin. Chem. Lett. 34 (2023) 107441.
[7] Y. Liu, Z. Tu, S.H. Chan, Int. J. Hydrogen Energy 47 (2022) 12698–12710.
[8] F. Dong, C. Wang, B. Wang, et al., J. Mater. Chem. A 11 (2023) 23106–23132.
[9] J. Chen, H. Chen, Y. Wang, et al., Chin. J. Catal. 42 (2021) 1297–1326.
[10] X. Zhang, T. Zhang, H. Chen, Y. Cao, Appl. Energy 286 (2021) 116481.
[11] H.Y. Lin, H.Y. Yuan, C. Sun, Angew. Chem. Int. Ed. 64 (2025) e202504212.
[12] X. Cheng, C. Wang, J. Zhang, et al., Chem. Eng. J. 439 (2022) 135387.
[13] J. Kim, S. Kang, K. Min, et al., Chem. Eng. J. 502 (2024) 158078.
[14] S. Mishra, J. Sharma, P. Upadhyay, V. Kulshrestha, J. Mater. Chem. A 12 (2024) 29854–29868.
[15] G. Wang, J.L. Li, H.L. Li, et al., Chin. Chem. Lett. 34 (2023) 107497.
[16] K. Zhang, L. Wu, M. Li, et al., Chin. Chem. Lett. 36 (2025) 111043.
[17] S.Y. Liu, X.L. Wang, Z.M. Su, et al., Sci. China Chem. 67 (2024) 862–868.
[18] Y. Wang, J. Yang, S. Liu, et al., Sci. China Chem. 67 (2024) 3299–3309.
[19] S. Zhang, X. Bai, S.X. Liu, et al., Chem. Commun. 59 (2023) 4312.
[20] J. Song, H. Lei, L. Lin, M. Sun, G. Zhu, Chem. Sci. 16 (2025) 6231–6239.
[21] C.F.J. Faul, Acc. Chem. Res. 47 (2014) 3428–3438.
[22] N. Ogiwara, T. Iwano, T. Ito, S. Uchida, Coord. Chem. Rev. 462 (2022) 214524.
[23] R.L. Liu, D.Y. Wang, G. Li, et al., Coord. Chem. Rev. 522 (2025) 216224.
[24] H.Y. Wang, D.D. Zhang, J.Y. Niu, et al., Chin. Chem. Lett. 35 (2024) 108486.
[25] Y. Chen, P.W. Cai, S.T. Zheng, et al., Chin. Chem. Lett. 35 (2024) 110552.
[26] Q.Q. Liu, Y.Z. Cui, H.Y. Zang, et al., Polyoxometalates 2 (2023) 9140036.
[27] B. Li, Q.Q. Liu, H.Y. Zang, et al., Angew. Chem. Int. Ed. 136 (2024) e202408096.
[28] B. Li, X.W. Ren, H.Y. Zang, et al., J. Am. Chem. Soc. 145 (2022) 2243–2251.
[29] W. Lei, P. Ma, J. Wang, et al., Inorg. Chem. 63 (2024) 20492–20500.
[30] J. Liu, Y. Kuang, Y.Q. Lan, et al., Angew. Chem. Int. Ed. 135 (2023) e202304728.
[31] S. Shishido, T. Ozeki, J. Am. Chem. Soc. 130 (2008) 10588–10595.
[32] X.X. Li, M.J. Hou, K.Z. Shao, et al., Nat. Commun. 14 (2023) 5025.
[33] S.Y. Liu, C. Qin, Z.M. Su, et al., Sci. China Chem. 67 (2024) 862–868.
[34] Y. Chu, X.H. Li, Chin. Chem. Lett. 36 (2025) 111012.
[35] S.S. Wang, G.Y. Yang, Chem. Rev. 115 (2015) 4893–4962.
[36] W.J. Liu, Y.Q. Lan, et al., ACS Appl. Mater. Interfaces 11 (2019) 7030–7036.
[37] B. Li, Q.Q. Liu, H.Y. Zang, et al., Chem. Commun. 59 (2023) 13446.
[38] X. Yu, Y.H. Gu, S. Yuan, et al., Dalton Trans. 53 (2024) 17902–17908.
[39] M. Yang, P. Ma, J. Niu, et al., Inorg. Chem. 62 (2023) 6467–6473.
[40] C. Chen, T. Li, J. Wang, et al., Fuel 378 (2024) 132855.
[41] S. Li, S. Ashraf, B. Wang, et al., ACS Appl. Mater. Interfaces 12 (2020) 22910–22916.
[42] M.L. Liu, J.M. Xu, Y.Q. Lan, et al., Tungsten 6 (2024) 454–464.
[43] P.M. Unnikrishnan, O. Basu, R. Nasani, S.K. Das, Dalton Trans. 54 (2025) 2166–2176.
[44] M.A. Spackman, P.G. Byrom, Chem. Phys. Lett. 267 (1997) 215–220.
[45] M.A. Spackman, D. Jayatilaka, Cryst. Eng. Comm. 11 (2009) 19–32.
[46] W. Ma, J. Jin, X. Huang, et al., Dalton Trans. 49 (2020) 3849–3855.